Journal of Electron Spectroscopy and Related Phenomena 256 (2022) 147139

Contents lists available at ScienceDirect

Journal of Electron Spectroscopy and Related Phenomena

journal homepage: www.elsevier.com/locate/elspec

A rate model approach for FEL pulse induced transmissions changes, saturable absorption, X-ray transparency and stimulated emission

Markus Hantschmann *, Alexander Föhlisch

Helmholtz-Zentrum Berlin, Institute for Methods and Instrumentation for Synchrotron Radiation Research, Germany
Universität Potsdam, Institut für Physik und Astronomie, Germany

ARTICLE INFO

Keywords:
Free-electron-laser science
RIXS at FELs
Stimulated scattering
Pulse induced transparency
Scattering breakdown

ABSTRACT

As the use of free electron laser (FEL) sources increases, so do the findings mentioning non-linear phenomena occurring at these experiments, such as saturable absorption, induced transparency and scattering breakdowns. These are well known among the laser community, but are still rarely understood and expected among the X-ray community and to date lack tools and theories to accurately predict the respective experimental parameters and results. We present a simple theoretical framework to access short X-ray pulse induced light–matter interactions which occur at intense short X-ray pulses as available at FEL sources. Our approach allows to investigate effects such as saturable absorption, induced transparency and scattering suppression, stimulated emission, and transmission spectra, while including the density of state influence relevant to soft X-ray spectroscopy in, for example, transition metal complexes or functional materials. This computationally efficient rate model based approach is intuitively adaptable to most solid state sample systems in the soft X-ray spectrum with the potential to be extended for liquid and gas sample systems as well. The feasibility of the model to estimate the named effects and the influence of the density of state is demonstrated using the example of CoPd transition metal systems at the Co edge. We believe this work is an important contribution for the preparation, performance, and understanding of FEL based high intensity and short pulse experiments, especially on functional materials in the soft X-ray spectrum.

1. Introduction

The past two decades have lead to a rapid establishment of free electron laser (FEL) applications for the utilization of ultra-fast and extremely bright photon sources in the extreme ultra-violet to hard X-ray photon regime at sources such as Fermi Elettra, Flash, SACLA, or LCLS, and with new sources such as XFEL or SwissFEL due to commence operation in the near future. These sources enable new experiments and impressive insights into the very heart of matter through techniques such as scattering before destruction [1], pump probe experiments utilizing different combinations of two color X-rays or optical pump-probe setups [2–4], and many more. To enable these experiments and insights, higher photon densities and shorter pulse lengths have been pushed, which also opened the experimental window into non-linear X-ray–matter interactions. There, a whole new world of effects has been observed and reported, including multiple photon absorption [5], stimulated scattering [2,6], saturable absorption [7] as well as parametric conversion [8]. These effects, however, are still unexpected and unaccounted for in the X-ray community, although, the field of optical laser science has long been familiar with these effects [9] and thus has established models to account for high pulse power light–matter interaction [10,11]. As X-ray experiments are often seen as the toolbox to gain new insights into the systems under investigation rather than insights into the nature of light–matter interactions, these new effects are delaying the extreme potential of ultra-fast X-ray science to enhance our knowledge in chemical reaction dynamics and pathways, heterogeneous catalysis, photosynthesis, and solid state phase transitions, for example. There have of course been efforts to create theories to handle these effects and to understand them in detail, utilizing various techniques from solving the Maxwell–Bloch equations [12], to a Maxwell–Liouville–von Neumann approach [6,13,14], and a rate-equation based approach [15,16]. Although these models are powerful and work well for their specific use case (presented for gas or cluster targets), they are also computationally demanding and need extensive expertise to be adapted to different systems. As FEL science moves towards more applied areas of physical and chemical sciences, this exceeds the scope of many experimental proposals.

* Corresponding author at: Helmholtz-Zentrum Berlin, Institute for Methods and Instrumentation for Synchrotron Radiation Research, Germany
E-mail addresses: Markus.hantschmann@gmail.com (M. Hantschmann), alexander.foehlisch@helmholtz-berlin.de (A. Föhlisch).

https://doi.org/10.1016/j.elspec.2021.147139
Received 14 November 2020; Received in revised form 3 April 2021; Accepted 16 October 2021
Available online 15 March 2022

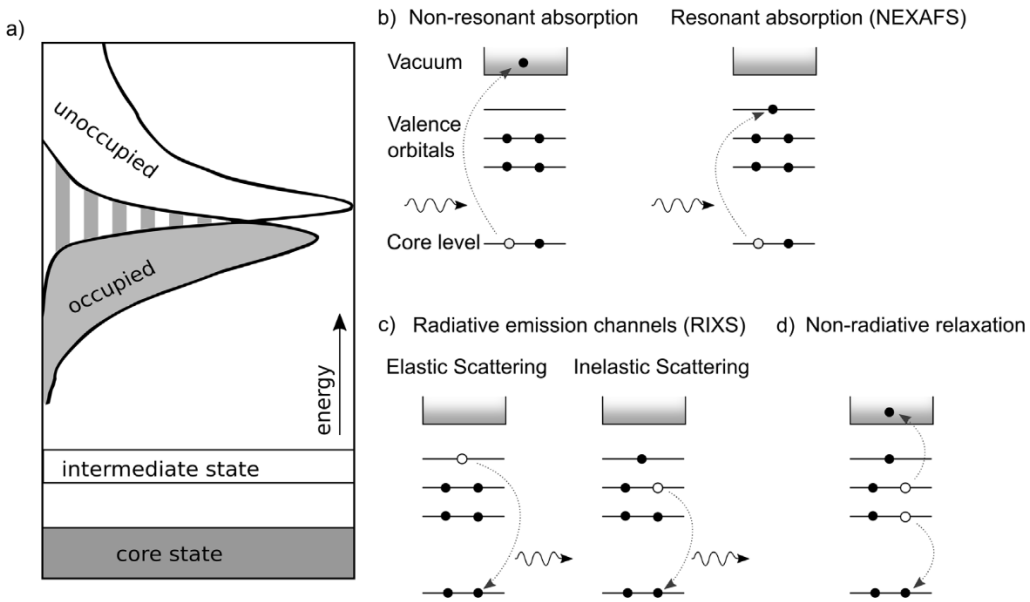

Fig. 1. (a) The initial setup of the model's sample system and the implemented energy conversion channels. In any X-ray–matter interaction, a core state electron is being excited into an absorption state or band, which then decays back into the core state, or into a non-radiative intermediate state. The absorption band can be partitioned into occupied and unoccupied states. The example displays a typical L-edge type of system, which we use for all following examples. (b/c/d) The typical relevant absorption (b), emission (c) and decay (d) processes in the soft X-ray regime.

Here it becomes obvious that we are still in need of a quick and simpler to use toolbox to get a realistic estimation of the expected interactions for varying experimental conditions, especially for functional materials with a high density of states (DOS) around the absorption edge. We decided to build up on the knowledge of optical laser science and transfer this to a simple and easy to expand toolkit that functions well for this type of soft X-ray–matter interaction experiments and can enable a fast window into high intensity soft X-ray FEL science. This paper is organized as follows: First, the rate model is introduced with its various aspects and relevant setup parameters including the intensity dependent cross sections and the density of state estimation for the absorption band. Secondly, the dynamics of a pulse transmission are being discussed with respect to the internal occupation changes, the intensity dependent rate changes, and the spectral effects of the individual channels. Lastly, the spectral changes of a transmitted pulse are investigated with their dependency on the incident pulse's energy, intensity, and the sample's density of states. The paper finishes with a comparison to the scattering breakdown observed by Chen et al. [17].

2. Theoretical approach

We start our model discussion from a well established set of rate equations whose derivations and applications can be found in for example [9,10,18]. The presented approach is based on a three band/state system containing a core state, an intermediate non-radiative decay state, and the absorption band, which is common in functional materials and can be partly occupied, as shown in Fig. 1(a). For simplicity, the core and the intermediate state are not energy resolved, i.e. from the core state, every state in the absorption band can be reached (compare Fig. 1b/c) and every state in the absorption band can decay into the core or intermediate state (compare Fig. 1c). The intermediate state works as a relaxation state for all non-radiative decay mechanisms. In the soft X-ray regime, this decay mechanism is dominated by the Auger decay. This implementation is different from simulations presented by Hatada and Di Cicco [15,16], as our model considers the DOS in the absorption band, thus enabling energy resolved information on spectral changes and spectroscopic features induced by the X-ray pulse. Furthermore, the model considers an intensity driven cross section as discussed by Patterson [19] and extended by Schreck et al. [20].

2.1. Rate equations

The basis of our rate equation system is the time evolution of the population number of the three bands and states (N_{Core}, N_{Band}, $N_{Intermediate}$), respectively, and their interaction channels (Fig. 1(b)–(d)). Following the textbook formalism [9], this leads to:

$$\frac{\partial N_{Core}(t)}{\partial t} = \sum^{E}[-R_{Abs}(E,t) + R_{Stim}(E,t) + R_{Spon}(E,t) + R_{Decay}(t)] \quad (1)$$

$$\frac{\partial N_{Band}(E,t)}{\partial t} = R_{Abs}(E,t) - R_{Stim}(E,t) - R_{Spon}(E,t) - R_{Aug}(E,t) \quad (2)$$

$$\frac{\partial N_{Intermediate}(t)}{\partial t} = R_{Aug}(t) - R_{Decay}(t) \quad (3)$$

The three levels can be populated or depopulated by the processes shown in Fig. 1(b)–(d), namely absorption R_{Abs}, spontaneous R_{Spon} and stimulated R_{Stim} emission, and non-radiative decay R_{Decay}, here given as the number of events at the given time and energy. The core state, as mentioned above, is energy independent in our model, therefore we sum over all energy channels to obtain the total population change. The core state in this model can be depopulated through absorption and repopulated through spontaneous emission, stimulated emission, and the decay of the intermediate states, respectively. The absorption band is implemented as an ensemble of states that can be partially occupied, as shown in Fig. 3. The absorption band is populated through absorption and depleted via stimulated emission, spontaneous emission, and Auger decay. As we simulate the transmission of short X-ray pulses of the order of femtoseconds in the soft X-ray regime, non-radiative decays are dominated by Auger decay (Fig. 1(d)), thus other non-radiative decays are not included in our current model. Therefore, the intermediate state can decay into the core state through non-radiative relaxation and can be populated through the absorption band via the Auger decay. With the exception of the decay from the intermediate state to the core state, all interactions are time and energy resolved. The interstate transition events are given by the following equations:

$$R_{Abs}(E,t) = I(E,t) \cdot \frac{\lambda A}{hc} \cdot \sigma_{abs}(E) \cdot f_{Abs}(E,t) \quad (4)$$

$$R_{Spon}(E,t) = I(E,t) \cdot \frac{\lambda A}{hc} \sigma_{Spon}(E) \cdot N_{Band}(E,t) \cdot f_{Spon}(E,t) \quad (5)$$

$$R_{Auger}(E,t) = I(E,t) \cdot \frac{\lambda A}{hc} \sigma_{Auger}(E) \cdot N_{Band}(E,t) \cdot f_{Aug}(E,t) \quad (6)$$

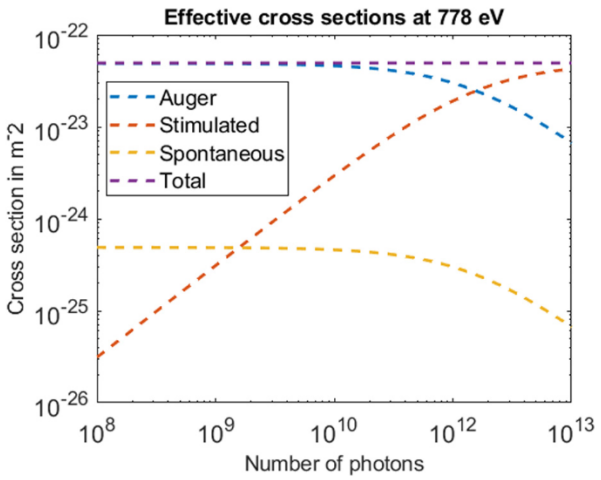

Fig. 2. An example of the decay cross sections used in our model, here for a photon pulse at 778 eV. Depending on the number of photons within a pulse, the distribution of decay cross sections changes, whilst the total decay cross section, equaling the total absorption cross section and the sum of all decay cross sections, stays constant. Towards higher photon numbers, the Auger and spontaneous cross sections are suppressed for the benefit of the stimulated cross section. The equations are based on the model developed by Schreck et al. [20] and have been implemented into our model.

$$R_{Stim}(E,t) = I(E,t) \cdot \frac{\lambda A}{hc} \sigma_{Stim}(E) \cdot N_{Band}(E,t) \cdot f_{Stim}(E,t) \tag{7}$$

$$R_{Decay}(t) = \frac{N_{intermediate}(t)}{\tau_{non-radiative}} \tag{8}$$

These event numbers depend mainly on three factors: first, the incident pulse $I(E,t)$ with the photon distribution in time and energy, second, the respective interaction cross sections $\sigma(E)$ or decay times τ as further discussed in the next section, and finally, the occupation factors $f(E,t)$ between the involved states. The incident pulse is taken in terms of total number of photons at a given energy and time, as shown in Eq. (11). The occupation factor f is given by the product of the relative occupations of the two involved states, for example, the occupation factor for absorption becomes the product of the occupied core state occupation and the available unoccupied absorption state occupation:

$$f_{abs}(E,t) = \frac{N_{Core}(t)}{max(N_{Core})} \cdot (1 - \frac{N_{Band}(E,t)}{max(N_{Band}(E,t))}) \tag{9}$$

The other variables have the usual meaning, with A being the incident pulse focus size. As our discussion evolves around the dynamics induced by very short pulses on the order of femtoseconds, and the non-radiative decay time scale is much longer, we assume $\tau_{non-radiative} = \infty$, thus eliminating non-radiative relaxation from the model system.

2.2. Decay cross sections

The decay cross sections are implemented as described by Schreck et al. [20], where the authors show how they can be determined from the total absorption cross section, the photon energy and the present photon field. More specifically, the total absorption cross section has to decay through one of the decay channels, thus the sum of decay cross sections has to equal the total absorption cross section:

$$\sigma_{Abs} = \sigma_{Aug} + \sigma_{Spon} + \sigma_{Stim} \tag{10}$$

The resulting cross section distribution for different photon numbers can be seen in Fig. 2, where they have been calculated for a 10 fs incident pulse with varying photon number at 788 eV. The maximum is given by the absorption cross section (violet line) at a given energy, but changes with the absorption cross section over the absorption band (compare Fig. 3 blue line). The distribution of decay cross sections is dependent on the energy and the total number of photons. As the sample is treated in a one-dimensional way, we treat the total number of photons present as the sum of all photons that have passed into the sample within a given time t. Therefore, the decay cross sections (compare Fig. 2) will initially start at the lower end of photon numbers and will stop changing when reaching the total number of photons within the pulse when the pulse has effectively been transmitted. This leads to a somewhat distorted decay behavior of our model after the pulse has passed. However, as we focus on the light-sample interaction during the pulse and not the sample recovery behavior, this should not pose an issue. As one can see in Fig. 2, the majority of the decay cross section is given by the Auger decay, which holds true for the soft X-ray regime, yet for higher photon energies, the majority of decays switches from Auger to spontaneous emission, as expected and shown in [20]. For increasing photon numbers, the photon field dependent stimulated cross section increases, thus suppressing the spontaneous and Auger decay cross sections. This concept is completely implemented into our model and a full derivation can be found in Schreck et al. [20].

The absorption cross section is commonly known for most sample systems, however as FEL pulses can saturate absorption and induce transparency [7,17,21], the absorption cross section may not be treatable like an interaction constant, but can change with the incident pulse intensity. These types of changes have been discussed by Stöhr et al. [22] for a 2-level system. It is possible to implement a time, intensity, or absorbed energy dependent change into the absorption cross section in our model. This affects all rates, as the decay rates depend on the absorption cross section for example through the opening of core level holes. We tested a factor decreasing and increasing the overall absorption cross section with the transmitted pulse intensity and found this to affect the timing (delay or accelerate) of the dynamics, but not the spectral position of the changes. Thus for the following, we do not implement this factor affecting the absorption cross section.

2.3. The incident pulse

For the incident pulse we used a Gaussian shaped light pulse in the time and energy regime. The pulse can be written in terms of intensity I or photon number N_{Photon} at a certain energy and time, as given in Eqs. (11), (12), respectively. Here I_0 is the incident intensity in $\frac{J}{cm^2 fs}$, with σ_t and σ_E being the time and energy width of the pulse, and A the focus size. The pulse can be shifted in the time domain using the time offset t_{Off}, and in energy using the energy offset E_{off}.

$$I(E,t) = I_0 \cdot exp\left(-\frac{1}{2} \cdot (\frac{t - t_{off}}{\sigma_t})^2\right) \cdot exp\left(-\frac{1}{2} \cdot (\frac{E - E_{off}}{\sigma_E})^2\right) \tag{11}$$

$$N_{Photon}(E,t) = I(E,t) \cdot \frac{\lambda A}{hc} \tag{12}$$

To simulate the spectral changes after transmission, we look at the time evolution of the transmitted pulse's photon numbers $Pulse_{trans}$ in time and energy (Eq. (13)), which depends on the incident pulse $I(E,t)$ and the two channels ($R_{Abs}(E,t)$ and $R_{Stim}(E,t)$) depleting and refilling photons.

$$\frac{\partial Pulse_{trans}(E,t)}{\partial t} = I(E,t)\frac{\lambda A}{hc} - R_{Abs}(E,t) + R_{Stim}(E,t) \tag{13}$$

For the model it is of course feasible to adapt the pulse to represent typical SASE patterns with multiple spikes at different energies and varying time delays, although they are not straightforward to compare as the occupation changes strongly depend on the spectral distribution of these SASE pulses. Hence for the demonstration of the model, we utilize Gaussian shaped pulses that vary in intensity, time, energy, and width.

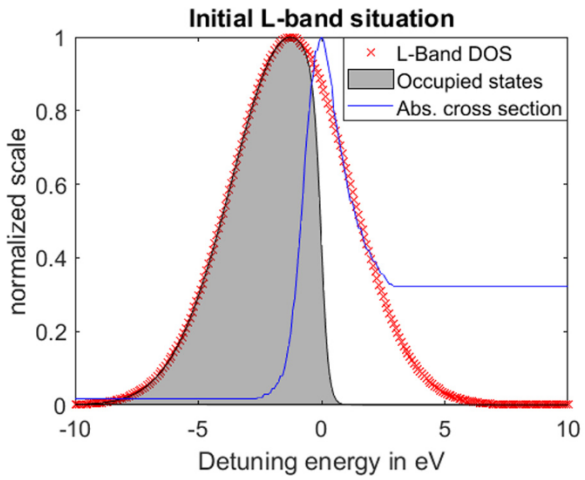

Fig. 3. Initial band occupation for a Co L-edge simulation. Width and distribution have been created to be comparable to [23] for Co through a Gaussian, convoluted with a Fermi–Dirac distribution. The gray area represents initially occupied states, while the white area represents free unoccupied states. The red curve indicates the available states at the given energy, while the blue curve gives the absorption cross section at the Co L-edge.

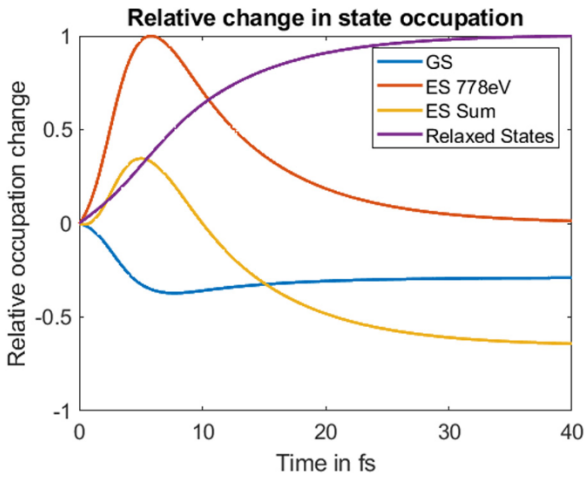

Fig. 4. The relative occupation change in the different states is shown for a 5 fs 2 eV FWHM pulse with an intensity of 10 mJ/(cm^{2}fs). As the pulse travels through the sample, the ground state (blue) occupation is converted into excited state or absorption band population (red and yellow). Over time, the Auger decay starts to occupy the intermediate relaxed states (purple), thus depopulating the majority of the excitation band and preventing it from recombining into the core hole ground state.

2.4. Absorption band DOS

To estimate the available states in the interaction region, we calculate the interaction volume from the sample dimensions and the pulse focus as $V_{interaction} = A \cdot d$, with the focal size A and the sample thickness d. Multiplying this with the atom density ρ_{Atom} yields an estimate for the number of atoms in the interaction volume. From this we get an estimate for the maximum number of states in the core level and the interaction band through the electron count of the respective orbital, i.e. times 2 for the core level and times the number of electrons n_e in the absorption band. This obviously leads to an initial occupation number of the core and interaction band which in turn enables to follow relative occupation changes. To account for the DOS in the absorption band around the edge, one can either take a full DOS for the initial distribution, or take an XES measurement as a measure of occupied states and an XAS measurement as a measure for unoccupied states in the absorption band. For most material systems, this information is well known, for example a Co L-edge is described in [23] and reproduced in Fig. 3. We approximate this distribution through a Gaussian distribution, reflecting the total number of states in the absorption band at the given energy, which then is multiplied with a Fermi–Dirac distribution, to get an initial distribution for occupied, unoccupied, and total available states at the different absorption edge energies, as displayed in Fig. 3. In our example, the gray area shows the initial occupation of states around the absorption edge, whereas the red line represents the available states at a given energy. For visualization, the absorption cross section, which has been adapted from [22] for the Co L-edge of a CoPd multi-layer, is shown in blue. For the ratio of occupied and unoccupied states, we found the ratio of electrons in the absorption band to be a rather good measure. For example for a Co L-edge, there are 7 out of 10 d-electrons, yielding a pre-occupation of 70% of the available states in the absorption band, which compares well to the situation measured for a Co film by Nillson et al. [23].

When discussing X-ray absorption or X-ray emission spectroscopy, the core hole screening effect and the Z+1 rule [24] have to be considered with different strengths for different material systems. As the RIXS process discussed here moves from an initial state via a transient state back to said initial state, and the dynamic effects connected to core hole screening occur for nearly filled bands in the ground state [25], which is not the case here, we consider the core hole screening to be negligible for the discussions below.

2.5. Occupation dynamics

Now we consider a Gaussian shaped pulse being transmitted through the described sample system. This results in an occupation dynamic, as displayed in Fig. 4. Here one can see how the incident pulse depopulates the ground state (blue) while increasing the occupation of the excited states in the absorption band, shown as a sum of all states (yellow) and a single state at the central resonance 778 eV (red). As time goes on, the excited states decay while reoccupying the ground state through stimulated and spontaneous emission and the intermediate relaxed state (purple) through Auger decay. In the following we do not consider a decay from the relaxed state back into the core hole ground state as we focus on the immediate pulse matter interaction and not on the slower relaxation behavior.

3. Model applications; CoPd multi-layer samples under short high intensity pulses

To illustrate how the model can be applied for short pulse high fluence X-ray spectroscopy experiments, we choose a typical transition metal Co L-Edge spectroscopic situation as described in [21], which has shown changes in transparency and scattering in past FEL experiments [17,21,26]. As the CoPd system has a high DOS around the Fermi level, we expect the impact of the DOS on the transaction rates to be high compared to other typical soft X-ray spectroscopic systems. We streamline the SASE pulses from typical FEL experiments by using a resonant Gaussian shaped pulse of variable intensity, energy and length, as this significantly simplifies the interpretation of our simulations and enables a much better understanding of the model's dynamics.

3.1. Transmission and induced transparency

In Fig. 5, the transmission of a resonant 2 eV FWHM pulse is shown for varying central pulse energies relative to the resonance (778 eV). The transmission is defined as the difference between the sum of all incident photons and the sum of all transmitted photons. The transmission for all pulses increases for higher incident pulse intensities, starting with a linear increase for lower incident intensities (inset) before slowly saturating towards (almost) full transparency at higher intensities. The general transmission increase is due to two reasons in the model. First,

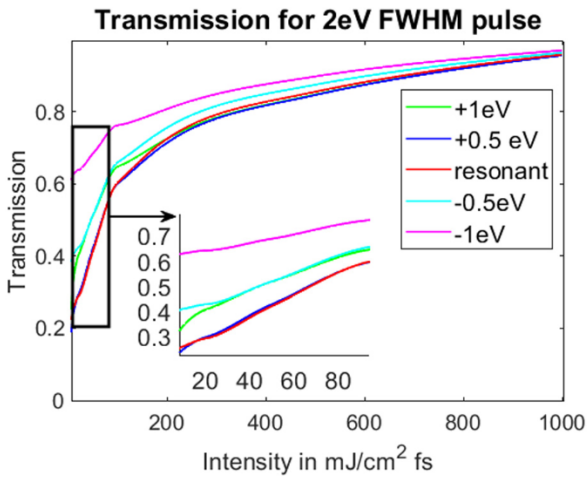

Fig. 5. Left: The transmission of an incident pulse is shown for a resonant (red) and detuned (other colors) 2 eV FWHM pulse. The resonant pulse (red) shows the lowest initial transmission, as most photons overlap with the majority of empty absorption band states, whereas the detuned pulses overlap with less available absorption band states (positive detuned, green and blue) or more already occupied states (negative detuned, cyan and pink). For low intensities (inset), all pulses show a linear transmission increase with increasing pulse intensity, but for higher intensities, the transmission converges towards an effectively fully transparent sample.

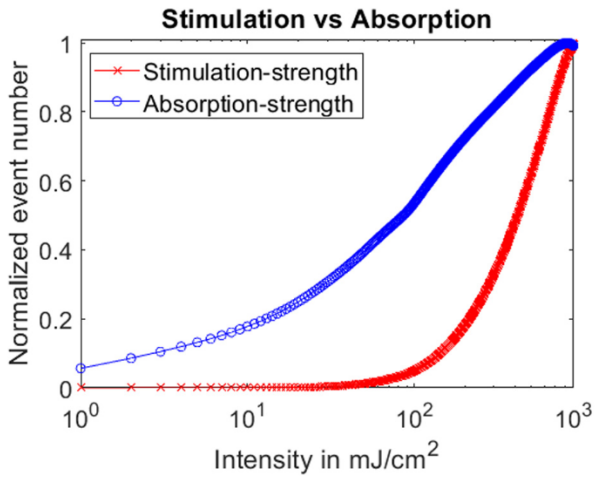

Fig. 6. The intensity dependent relative amount of stimulated and absorption events, respectively, simulated for a 2 fs long resonant pulse of 2 eV FWHM. The absorption increases with the incident pulse intensity, whereas the stimulation only starts to set in for high intensities, but then amplifies rapidly. The event numbers have been normalized to the maximum number of events for each channel, respectively. This is done for easier visualization of the two event numbers, as absorption is occurring at far higher rate than the stimulation. The exact strength of the two channels depends on a number of factors. This image should visualize the trend between the linear increase in absorption and the non-linear increase in stimulated events.

the ground state population gets depleted more strongly with increasing intensity, which reduces the probability of further absorptions through the population factor f. Second, the higher the incident intensity gets, the higher becomes the probability for stimulated emission events, which work as a counterbalance to absorption as they 'add' photons to the transmitted pulse, thus effectively increasing the transparency. The transparency depends on the incident photon distribution, being higher for a pulse that has reduced overlap with unoccupied absorption band states, which is the case for all detuned pulses. For a +1 eV detuned pulse (pink), the photon distribution only overlaps by about 30% with empty absorption band states (as illustrated by the white area in Fig. 3), therefore the transparency at low incident pulse intensities is approximately doubled compared to the resonant pulse. The resonant pulse (red) and the 0.5 eV positively detuned pulse (blue) have almost the same transparency evolution, as they both highly overlap with the absorption cross section, which reflects the width of the strongest absorption area (compare with the absorption cross section (blue) in Fig. 3).

3.2. Intensity dependent absorption and stimulation

To compare the absorption and stimulation channel, Fig. 6 shows the respective number of events, which is defined as the sum of all channel events, here calculated for a 2 fs long resonant pulse. As the pulse intensity increases, so do the two optical channels, however, while the absorption increases steadily with increasing intensity, the stimulation only starts to kick in above 100 mJ/cm^{2}fs. This effect of the superlinear increase in stimulated emission with higher intensity is analogous to the light-versus-current characteristic in, for example, semiconductor lasers (Ref. [27] Figs. 5 and 6). Also, the respective events do not occur at the same photon energies, which leads to an asymmetric sample reaction in state changes, as will be discussed in more detail in Section 3.3. But first, we compare the spectral evolution of the absorption and stimulation channels, which are shown in Fig. 7 and Fig. 8 respectively. Since the spectral changes are normalized, only relative changes can be seen here. The spectral distribution of absorption events shifts from the higher end of the absorption edge towards the lower end, thus occurring more frequently in spectral areas with more pre-occupied L-band states. Also, the overall absorption distribution is more pronounced and steeper around 1–2 eV, however this is a feature of the normalization, as for increasing numbers of absorption events this quenches the lower numbers. Note that this effect is not observable at the lower energy end of the distribution, hinting to an asymmetric absorption behavior, which is to be expected given the asymmetric pre-occupation of the absorption band (compare white and gray area in Fig. 3). For the spectral distribution of stimulation events, the shift only occurs in an asymmetric way towards higher intensities. Comparing Figs. 7 and 8, one can see that the stimulation distribution is shifted to lower energies compared to the absorption distribution. As these two have the opposite effect on the transmitted photons (i.e. stimulation adds photons to the transmitted pulse while absorption removes them), this leads to a change in the transmitted photon distribution, which is discussed in the following section.

3.3. Spectral changes in transmission

To compare the strength of these two channels at the respective photon energies, we compare the relative difference given by $\frac{\#R_{Abs}(E)-\#R_{Stim}(E)}{\#R_{Abs}(E)}$, which gives a measure for the relative change of the linear transmission at the given photon energies for this setup. An example for the resulting relative differences is shown in Fig. 9 for a resonant pulse of 2 eV FWHM and varying incident intensities. The overall difference increases as the incident intensity increases and, therefore, the strength of the stimulation channel grows. The asymmetric change is obvious and can be separated into two different areas. The first is the main peak, which coincides with the bulk of the pre-occupied L-band states and hence with an area of less absorptions. This area can, for higher intensities, contribute to an increased transmission and ultimately for an effective increase in the number of photons transmitted even above the incident photon count. This area would give rise to the amplification of the incident pulse through stimulated emission, very much like a typical semiconductor optical amplifier. The main surprise here is how far below the resonance this area occurs. In this case the maximum change is around −2 eV.

The second interesting relative difference is the plateau-like reduction just around the resonant energy. This is caused by the overlap of the stimulated distribution and the absorption distribution, as shown in

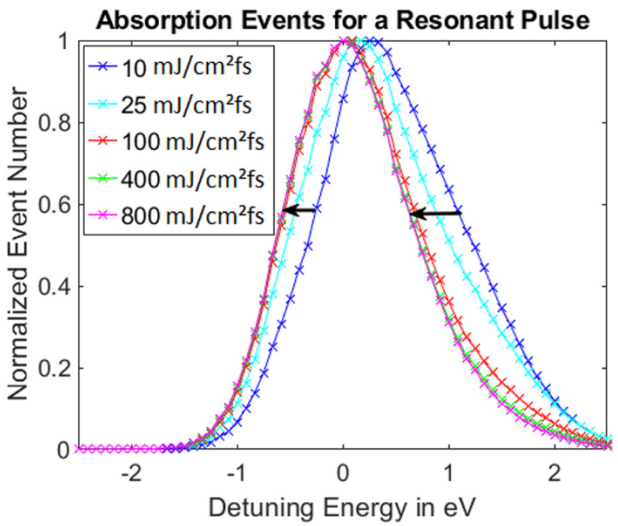

Fig. 7. Relative spectral changes of the absorption for different incident pulse intensities. The change in the spectral absorption distribution shifts towards lower energies with increasing incident intensity until it saturates at about 400 mJ/(cm²fs) (green). The absorption distribution also narrows, as can be seen from the falling edge at the high intensity curves.

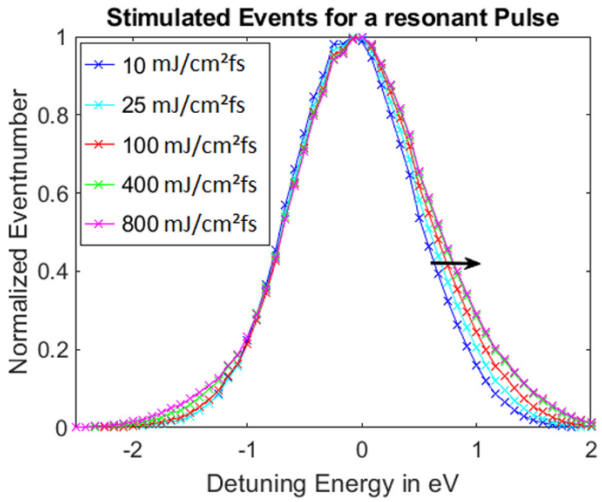

Fig. 8. Relative spectral changes of the stimulated channel for different incident pulse intensities. The stimulated distribution does not shift, but broadens with increasing incident intensity towards higher incident intensities, thus working as a counterweight to the absorption distribution shift through the increased depopulation of excited states through stimulated emission.

Figs. 8 and 7, counteracting each other with respect to the transmission. The stimulated emission is far weaker than the absorption, but still increases the transmitted photons in these spectral areas, resulting in an effective increase in transmitted photons. This reduction in absorption can be measured in transmission experiments and has indeed been reported by Chen et al. who measured the transmission of a CoPd thin film L-edge spectra for ultra-fast short X-ray pulses [17]. However, as reported by Highley et al. effects beyond stimulated scattering such as for example electron cascades change the influence of stimulated scattering on these systems [26].

Fig. 10 shows the effect of detuning on the described difference for a 200 mJ/cm²fs pulse of 2 eV FWHM, with the detuning being an energy shift of the incident pulse with respect to the resonance at 778 eV. As mentioned in Section 3.1, the resonant (yellow) and slightly positively detuned (+0.5 eV red) pulse examples are almost identical, as they both

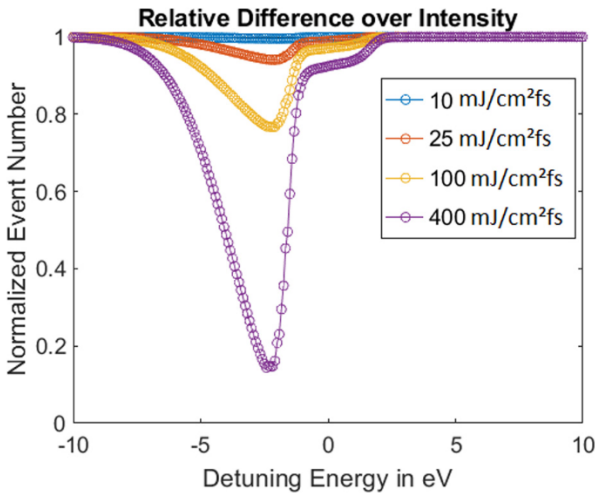

Fig. 9. The relative differences of the stimulated and absorption channel strengths are shown as the difference of stimulated and absorption events normalized by the number of absorption events. One can see how an increase in intensity increases the relative difference of the two channels and thus changes the transmitted photon distribution. I.e. the sample becomes more transparent for photon energies where the relative difference is lower, eventually resulting in an increased transmission that can become higher than 1.

have a very high overlap with the absorption cross section. This leads to a higher activity in absorption, increasing the number of occupied L-band states, while depopulating the core levels and ultimately leading to more stimulated emission and thus a higher relative difference. The other detuned pulses exhibit a lower amount of absorption events, but the more relevant feature is the fact that the main peak follows the pulse detuning direction. However, as the detuning from the resonance for all examples is larger than the shift, while the highest difference is well below the highest photon peak, the total relative difference has to be understood as a convolution of incident photon distribution, pre-occupation distribution, the stimulated and absorption distribution, and the effective transmission. One could argue that the Auger decay strength must also have an effect on the spectral difference, as it will also occur in an asymmetric way, since the L-band occupation is higher for the pre-occupied area of the absorption band thus leading to more Auger decays in our model. However, we found this to only have a minor impact on the differences, as the Auger decay works like a counter-effect against the stimulated emission through the depletion of excited states, but in turn gets suppressed by the stimulated emission at higher intensities (compare Fig. 2). Also this effect is already included in the stimulated distribution here, as Auger decay and stimulated emission are linked through their respective cross sections. The two spectral features in Figs. 9 and 10 are experimentally observable as a decrease in absorption, but under different conditions: As the main difference (around −2 eV detuning energy) strongly depends on the tuning of the incident pulse, this will be easier to observe under monochromatic conditions. Conversely, the plateau-like decrease around 0 to 2 eV is robust to the incident pulse energy distribution and should thus be observable in SASE operation.

3.4. Transmitted photon distribution and stimulated signature

The previously discussed changes in the internal cross channel rates of course result in differences in the transmitted photon distribution, which are shown in Fig. 11 and Fig. 12, respectively. Fig. 11 shows a photon difference map between the transmitted pulse and the incident pulse ($N_{photon}(transmitted)(E) - N_{photon}(incident)(E)$) compare Eq. (12), which has been normalized to values between 1 and −1 for better visualization. The change in the transmitted spectral distribution can

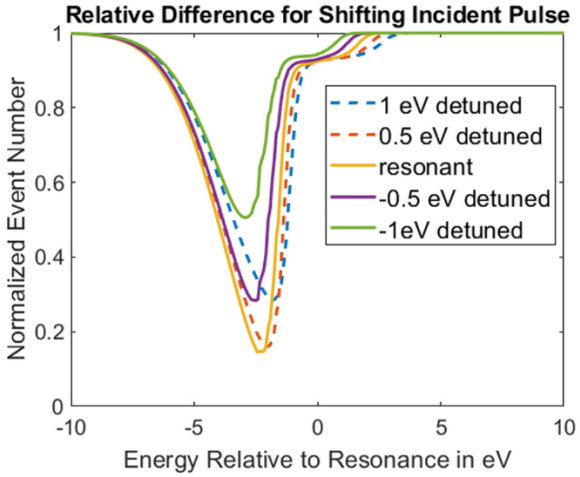

Fig. 10. The relative differences of the stimulated and absorption channel strengths are shown as the difference of stimulated and absorption events normalized by the number of absorption events. One can see the how detuning of the incident pulse for an intensity of 200 mJ/(cm^{2}fs) changes this relative difference. The maximum of the difference follows the detuning direction, while the overall difference reduces for both detuning directions. Note that there is a plateau-like area around the resonance that does not change in strength for different detuned pulses. This effectively reduces the observed absorption while increasing the transmitted photons at these energies compared to lower incident intensity pulses.

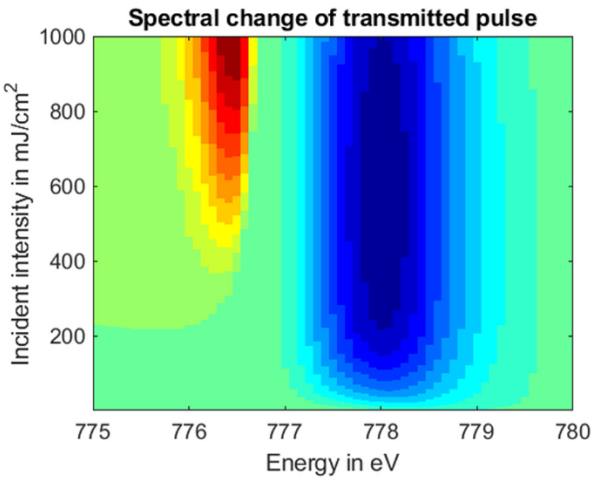

Fig. 11. The image shows a difference map of the transmitted number of photons compared to the incident number of photons at the given energy. The map has been calculated for a resonant 2 eV FWHM pulse and is normalized to changes between 1 (red) and −1 (blue) to visualize the stimulated features appearance. The red feature corresponds to a higher photon number after transmission, whereas the blue feature corresponds to the typical expected absorption edge. The stimulated feature appears 1.5 eV below the absorption edge.

be compared for rising intensities. The blue feature corresponds to the absorption edge and a reduction in transmitted photons, whereas the red feature corresponds to an increase in transmitted photons compared to the incident pulse. Note that the stimulated edge occurs 1.5 to 2 eV below the resonant absorption edge (778 eV). Fig. 12 shows cuts of the un-normalized photon differences, bringing the rise through stimulation in relation to the dip through absorption. The image displays changing intensity from lower intensity (blue) to higher intensity (red). With rising intensity, more photons get absorbed, leading to a deeper absorption edge but also a rise in the stimulated feature, as shown in the inset. This results in a steeper low energy flank and ultimately a reduction in absorption edge width. However, the overall absorption overshadows the amount of stimulated photons.

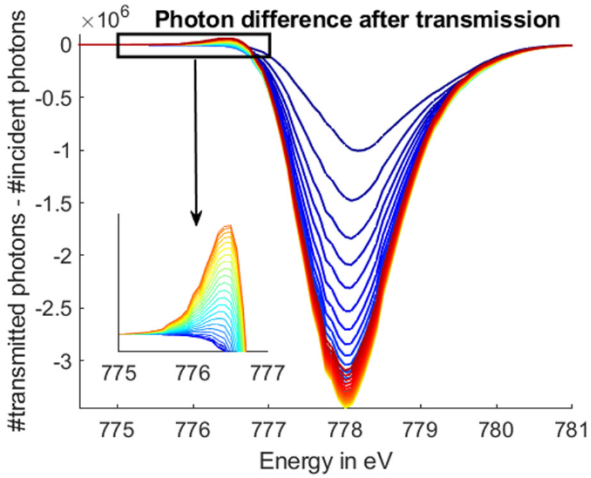

Fig. 12. The un-normalized data set for the photon difference after transmission, displayed from low (blue) to high (red) intensity, brings the increase in transmitted photons in relation to the decrease through absorption. As the absorption edge becomes deeper, the stimulated edge rises, resulting in a reduction in the (low energy) width of the absorption edge and a steeper low energy flank.

As discussed above, the position of the stimulated edge is dominated by the initial band structure and mostly affected by the position of the incident pulse through the overlap with pre-occupied states and the overlap with the incident intensity. Therefore, a SASE pulse with for example two spikes, one on the absorption edge and one 2 eV below the edge, should induce a strong stimulation for the lower energy spike. This of course becomes feasible to achieve with the new emerging two color FEL conditions [28] at various FEL sources around the world, which will strongly increase the control over the experimental conditions in FEL experiments compared to SASE operation.

3.5. Stimulation impact on scattering: Scattering breakdown

A last aspect to be discussed is the effect increased stimulated emission has on X-ray scattering. As stimulated emission emits in the pulse (forward) direction and reduces the amount of spontaneous decays with increasing intensity, it also reduces the scattering signal, which is primarily caused by these spontaneous decays. This effect quenches the pulse in the forward direction, increasing the transmission (compare Section 3.1) and reducing the 360° scattering. In Fig. 13, the blue curve shows the fraction stimulated emission takes from the total amount of decay events for a varying incident intensity of a 2 eV FWHM resonant pulse. As discussed before, the fraction of stimulated emission increases rapidly with increasing incident intensity, while suppressing the Auger and the spontaneous decay channel. The increase of stimulated events correlates with the measured decrease in diffraction contrast by Chen et al. [17] (which is for comparison shown in orange).

4. Conclusion and outlook

We have presented a rate model approach to simulate the interaction of FEL pulses with solid sample systems in order to understand the impact of effects such as stimulated scattering, induced transparency, and scattering breakdown in the soft X-ray spectrum. The model is easily adaptable to different material systems, especially solid state systems, includes intensity dependent cross sections, and the DOS of the absorption band. Although the presented model is strongly simplified compared to full quantum mechanical treatments, our approach is capable of reproducing the impact intensity-driven stimulated emission in FEL experiments has on scattering, spectroscopy, and transmission, while being computationally efficient and more quickly to perform.

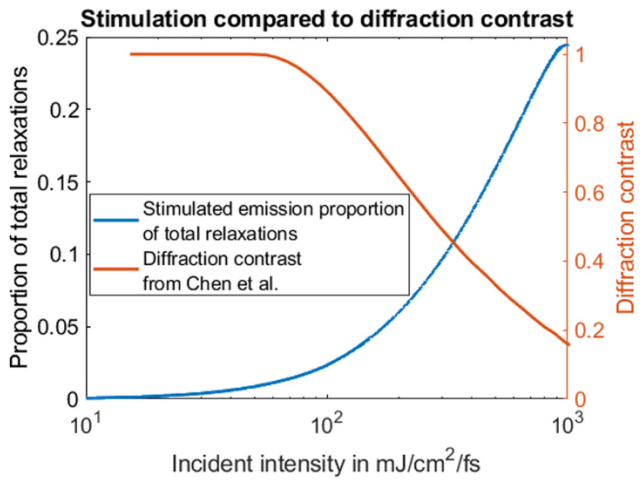

Fig. 13. This figure shows a comparison of the diffraction contrast measured by Chen et al. [17] (orange) to the proportion of stimulated decays as a fraction of the total occurring decays for a resonant 2 eV FWHM pulse and varying incident intensity (blue). The decrease in diffraction contrast correlates extraordinarily well with our calculation of increasing stimulated emission events, which corresponds to an increase in forward transmission of light at the cost of scattered (i.e. spontaneously emitted) light.

Based on this model, we simulated the transmission of Gaussian shaped pulses through a CoPd multilayer thin film, which has a high DOS around the L-edge and has been demonstrated to show non-linear behavior. We have presented how the interplay of the DOS and the pulse's energy and intensity drive the pulse-sample interaction in this system, and have demonstrated how induced transparency develops with intensity dependent absorption and stimulation rates, inducing an increase in transmission in the sample system. Furthermore, we have shown that the spectral distribution of absorption and stimulation events occur at different energies, thus inducing an asymmetric photon distribution change during transmission. This asymmetric behavior has been investigated in detail with respect to the incident pulse's intensity and energy, resulting in two key findings: first, a decrease in absorption on the main absorption resonance, which is in accordance with recent experimental findings, and secondly, the appearance of an increase in transmission 1–2 eV below the absorption edge dominated by stimulated emission. This stimulated feature can lead to an amplification of the incident pulse in a narrow spectral range, but is highly dependent on the incident pulse's energy, thus only being observable under very controlled experimental conditions. Lastly, we have compared the increase of stimulated events at higher incident pulse intensities with the experimentally observed decrease in diffraction contrast and conclude that the increase in stimulated emission events leads to a decrease in scattering events. We believe this paper is a strong contribution to the understanding and preparation of future FEL based soft X-ray experiments on solid sample targets and could help to paint a pathway towards controlled stimulated RIXS experiments. The data and scripts that support the findings of this study are available from the corresponding author upon reasonable request.

Acknowledgments

We want to acknowledge support by European Research Council Advanced Grants 2014 Advanced Investigator Grant 669531 "Beating Complexity through Selectivity: Excited State Dynamics from Anti-Stokes and Non-Linear Resonant Inelastic X-ray Scattering" under the Horizon 2020 European Union Framework Program for Research and Innovation as well as the G-ISRR, Helmholtz-Zentrum Berlin and the PhD completion scholarship of the University of Potsdam graduate school.

Appendix A. Supplementary data

Supplementary material related to this article can be found online at https://doi.org/10.1016/j.elspec.2021.147139.

References

[1] H.N. Chapman, A. Barty, M.J. Bogan, S. Boutet, M. Frank, S.P. Hau-Riege, S. Marchesini, B.W. Woods, S. Bajt, W.H. Benner, et al., Femtosecond diffractive imaging with a soft-X-ray free-electron laser, Nat. Phys. 2 (12) (2006) 839–843.
[2] M. Beye, S. Schreck, F. Sorgenfrei, C. Trabant, N. Pontius, C. Schüßler-Langeheine, W. Wurth, A. Föhlisch, Stimulated X-ray emission for materials science, Nature 501 (7466) (2013) 191–194.
[3] R.M. Jay, J. Norell, S. Eckert, M. Hantschmann, M. Beye, B. Kennedy, W. Quevedo, W.F. Schlotter, G.L. Dakovski, M.P. Minitti, et al., Disentangling transient charge density and metal–ligand covalency in photoexcited ferricyanide with femtosecond resonant inelastic soft X-ray scattering, J. Phys. Chem. Lett. 9 (12) (2018) 3538–3543.
[4] S. Gerber, S.-L. Yang, D. Zhu, H. Soifer, J. Sobota, S. Rebec, J. Lee, T. Jia, B. Moritz, C. Jia, et al., Femtosecond electron-phonon lock-in by photoemission and X-ray free-electron laser, Science 357 (6346) (2017) 71–75.
[5] N. Rohringer, D. Ryan, R.A. London, M. Purvis, F. Albert, J. Dunn, J.D. Bozek, C. Bostedt, A. Graf, R. Hill, et al., Atomic inner-shell X-ray laser at 1.46 nanometres pumped by an X-ray free-electron laser, Nature 481 (7382) (2012) 488–491.
[6] C. Weninger, M. Purvis, D. Ryan, R.A. London, J.D. Bozek, C. Bostedt, A. Graf, G. Brown, J.J. Rocca, N. Rohringer, Stimulated electronic X-ray Raman scattering, Phys. Rev. Lett. 111 (23) (2013) 233902.
[7] H. Yoneda, Y. Inubushi, M. Yabashi, T. Katayama, T. Ishikawa, H. Ohashi, H. Yumoto, K. Yamauchi, H. Mimura, H. Kitamura, Saturable absorption of intense hard X-rays in iron, Nat. Commun. 5 (1) (2014) 1–5.
[8] S. Shwartz, R. Coffee, J. Feldkamp, Y. Feng, J. Hastings, G. Yin, S. Harris, X-ray parametric down-conversion in the Langevin regime, Phys. Rev. Lett. 109 (1) (2012) 013602.
[9] H. Statz, G. DeMars, Transients and oscillation pulses in masers, in: Quantum Electronics, 1960, p. 530.
[10] C. Hantschmann, P.P. Vasil'ev, S. Chen, M. Liao, A.J. Seeds, H. Liu, R.V. Penty, I.H. White, Gain switching of monolithic 1.3 μm InAs/GaAs quantum dot lasers on silicon, J. Lightwave Technol. 36 (18) (2018) 3837–3842.
[11] M. Sugawara, H. Ebe, N. Hatori, M. Ishida, Y. Arakawa, T. Akiyama, K. Otsubo, Y. Nakata, Theory of optical signal amplification and processing by quantum-dot semiconductor optical amplifiers, Phys. Rev. B 69 (23) (2004) 235332.
[12] Y.-P. Sun, J.-C. Liu, C.-K. Wang, F. Gel'mukhanov, Propagation of a strong x-ray pulse: pulse compression, stimulated raman scattering, amplified spontaneous emission, lasing without inversion, and four-wave mixing, Phys. Rev. A 81 (2010) 013812, http://dx.doi.org/10.1103/PhysRevA.81.013812, https://link.aps.org/doi/10.1103/PhysRevA.81.013812.
[13] N. Rohringer, R. London, Atomic inner-shell X-ray laser pumped by an X-ray free-electron laser, Phys. Rev. A 80 (2009) 013809, http://dx.doi.org/10.1103/PhysRevA.80.013809, https://link.aps.org/doi/10.1103/PhysRevA.80.013809.
[14] C. Weninger, N. Rohringer, Stimulated resonant X-ray Raman scattering with incoherent radiation, Phys. Rev. A 88 (2013) 053421, http://dx.doi.org/10.1103/PhysRevA.88.053421, https://link.aps.org/doi/10.1103/PhysRevA.88.053421.
[15] K. Hatada, A. Di Cicco, Modeling saturable absorption for ultra short X-ray pulses, J. Electron Spectrosc. Relat. Phenom. 196 (2014) 177–180.
[16] K. Hatada, A. Di Cicco, Modeling non-equilibrium dynamics and saturable absorption induced by free electron laser radiation, Appl,. Sci. 7 (8) (2017) 814.
[17] Z. Chen, D. Higley, M. Beye, M. Hantschmann, V. Mehta, O. Hellwig, A. Mitra, S. Bonetti, M. Bucher, S. Carron, et al., Ultrafast self-induced X-ray transparency and loss of magnetic diffraction, Phys. Rev. Lett. 121 (13) (2018) 137403.
[18] J. Carroll, J. Whiteaway, D. Plumb, Distributed Feedback Semiconductor Laser, 1999, p. 409.
[19] B.D. Patterson, SLAC, Resource Letter on Stimulated Inelastic X-ray Scattering at an XFEL, 2010, http://dx.doi.org/10.2172/992898.
[20] S. Schreck, M. Beye, A. Föhlisch, Implications of stimulated resonant X-ray scattering for spectroscopy, imaging, and diffraction in the regime from soft to hard X-rays, J. Modern Opt. 62 (Suppl. 2) (2015) S34–S45.
[21] B. Wu, T. Wang, C. Graves, D. Zhu, W. Schlotter, J. Turner, O. Hellwig, Z. Chen, H. Dürr, A. Scherz, et al., Elimination of X-ray diffraction through stimulated X-ray transmission, Phys. Rev. Lett. 117 (2) (2016) 027401.
[22] J. Stöhr, A. Scherz, Creation of X-ray transparency of matter by stimulated elastic forward scattering, Phys. Rev. Lett. 115 (10) (2015) 107402.
[23] A. Nilsson, J. Stöhr, T. Wiell, M. Aldén, P. Bennich, N. Wassdahl, M. Samant, S. Parkin, N. Mårtensson, J. Nordgren, et al., Determination of the electronic density of states near buried interfaces: Application to Co/Cu multilayers, Phys. Rev. B 54 (4) (1996) 2917.
[24] A. Föhlisch, J. Hasselström, P. Bennich, N. Wassdahl, O. Karis, A. Nilsson, L. Triguero, M. Nyberg, L. Pettersson, Ground-state interpretation of x-ray emission spectroscopy on adsorbates: CO adsorbed on Cu (100), Phys. Rev. B 61 (23) (2000) 16229.

[25] A. Föhlisch, Probing Molecular Adsorbates with Core-Level Spectroscopies: Electronic Structure and Bonding Models.

[26] D.J. Higley, A.H. Reid, Z. Chen, L. Le Guyader, O. Hellwig, A.A. Lutman, T. Liu, P. Shafer, T. Chase, G.L. Dakovski, et al., Femtosecond X-ray induced changes of the electronic and magnetic response of solids from electron redistribution, Nat. Commun. 10 (2019).

[27] K. Srinivasan, M. Borselli, O. Painter, A. Stintz, S. Krishna, Cavity Q, mode volume, and lasing threshold in small diameter AlGaAs microdisks with embedded quantum dots, Opt. Express 14 (3) (2006) 1094–1105, http://dx.doi.org/10.1364/OE.14.001094, http://www.opticsexpress.org/abstract.cfm?URI=oe-14-3-1094.

[28] T. Hara, Y. Inubushi, T. Katayama, T. Sato, H. Tanaka, T. Tanaka, T. Togashi, K. Togawa, K. Tono, M. Yabashi, et al., Two-colour hard X-ray free-electron laser with wide tunability, Nat. Commun. 4 (1) (2013) 1–5.